Behaviors of Sr_2IrO_4 Sample Synthesized under the Magnetic Field with 9 T

GE Min†, ZUO Ming, TAN Shun, ZHANG Yuheng

Hefei National Laboratory for Physical Sciences at the Microscale, University of Science and Technology of China, Hefei 230026, *China*

Received date: 2019-08-06; accepted date: 2019-08-06

【Abstract】 Sr_2IrO_4 has been successfully synthesized under the magnetic field with 9 T, and the structural and magnetic properties were characterized. Although its structure and crystal lattice are the same with the sample synthesized under 0 T, HRTEM reveals that the distribution of electron cloud is changed. The increased density of states in the dark regions leads to the differences in magnetism from the sample synthesized under 0 T. Our finding indicates that the magnetic field of 9 T could be more favorable to the growth of pure phase.

Keywords: Sr_2IrO_4, HRTEM, magnetism

PACS: 7340Rw, 7530Et

DOI: 10.13380/j.ltpl.2019.03.001

Reference method: GE Min, ZUO Ming, TAN Shun, ZHANG Yuheng, Low. Temp. Phys. Lett. **41**,0153 (2019)

在 9 T 磁场中合成 Sr_2IrO_4 样品的物理性质研究*

葛敏†,左鸣,谭舜,张裕恒

中国科学技术大学合肥微尺度物质科学国家研究中心,合肥 230026

收稿日期:2019-08-06;接收日期:2019-08-06

【摘要】 我们在 9 T 的磁场下成功合成了 Sr_2IrO_4 样品,并且研究了它的结构和磁性.尽管样品的晶体结构与在零场下合成的样品相比没有改变,高分辨透射电镜像显示出电子云的分布发生了变化.在暗区,态密度增强引起了样品的磁性发生改变.我们提出 9 T 的强磁场有利于生长出更纯相的样品.

关键词: Sr_2IrO_4, HRTEM, 磁性

PACS: 7340Rw, 7530Et

DOI: 10.13380/j.ltpl.2019.03.001

* Project supported by the National Natural Science Foundation of China through Grant nos. 11204288.

† gemin@ustc.edu.cn

1 Introduction

Sr_2IrO_4 is a hot-spot in strong correlated physics which is primarily driven by strong spin-orbit coupling (*SOC*)[1], and it has been deeply investigated in the last few years[2]. Our previous work find that both of the macro- and micro-magnetism exhibit interesting behaviors below 40 K, which are induced by the variation of Ir-O-Ir bond angle below 40 K[3]. To understand the physical properties of Sr_2IrO_4 and to find a way of tuning its competing interactions, experimental studies of chemical doping[4-11], and high pressure[12] have been recently conducted. The novel magnetism of the system has attracted great attention, but there are still some problems to be solved such as the influence of high magnetic field when synthesizing Sr_2IrO_4. Considering the features of spin canted structure and strong spin-orbit coupling in Sr_2IrO_4, sintering magnetic field may have some impacts on the formation of magnetic structure, and this research has not been involved yet. Therefore, it is necessary to study the physical properties of Sr_2IrO_4 which was sintered under high magnetic field.

In this work, we investigate the sample Sr_2IrO_4-9 T which was synthesized under the magnetic field of 9 T, by the X-ray diffraction (XRD), high-resolution transmission electron microscopy (HRTEM), infrared (IR) and measurements of macroscopic magnetism. We also study the sample Sr_2IrO_4-0 T which was synthesized under the magnetic field of 0 T for comparison. The spatial conditions and growth parameters are the same for these two samples, except that the sintering magnetic field is different. Our experimental results give an important finding that the structure and crystal lattice of Sr_2IrO_4-9 T are the same with Sr_2IrO_4-0 T, but the distribution of electron clouds is changed. Thus, the magnetism shows some different behaviors from Sr_2IrO_4-0 T.

2 Experiment

Polycrystalline sample of Sr_2IrO_4-0 T was synthesized under the magnetic field of 0 T as reported previously[3]. The same starting materials were mixed and heated under the magnetic field of 9 T. It is emphasized that both of them were calcined in the same position of the same furnace and their growth was completed in the same procedure for comparison.

Structure and phase purities were checked by the X-ray diffraction at room temperature, and single phase patterns were obtained. The magnetization was measured by a Magnetic Property Measurement System (Quantum Design MPMS 7T-XL) with a superconductive quantum interference device (SQUID). High-resolution transmission electron microscopy images were performed on JEOL-2010 transmission electron microscope at 200 kV. The electron spin resonance measurements were performed at 9.40 GHz using a BRUKEREMX plus 10112 spectrometer equipped with a continuous He gas-flow cryostat in the temperature region of 2-300 K by sweeping the magnetic field. The IR spectra were performed at various temperature from 300 K to 5 K.

3 Results and Discussion

X-ray diffraction patterns of Sr_2IrO_4 which were synthesized under the magnetic field of 0 T and 9 T show no difference between them, as depicted in Fig. 1. Thus, the lattice structure is not changed and they belong to the same space group of $I4_1/acd$. It is worth noting that the experimental results of Sr_2IrO_4-0 T are in good agreement with the physical properties of Sr_2IrO_4 which we obtained in our previous work[3].

Fig. 2 (a) gives the high-resolution transmission electron microscopy (HRTEM) image which consists of the (1 1 6) and (0 0 8) planes in Sr_2IrO_4-9 T sample. A new finding is given that some dark regions appear in Fig. 2 (a).

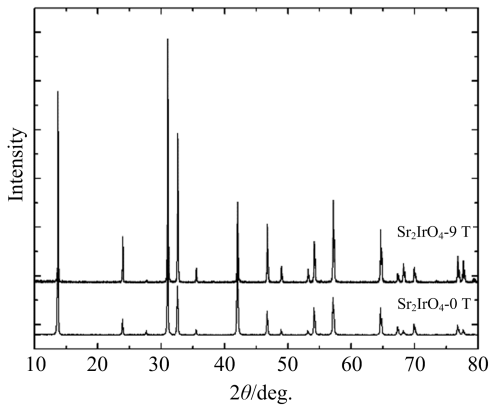

Fig. 1 Powder X-ray diffraction (XRD) patterns for Sr_2IrO_4-0 T and Sr_2IrO_4-9 T sample at room temperature

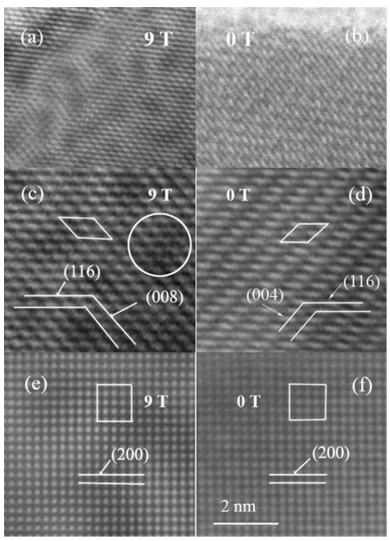

Fig. 2 (a) The HRTEM image which consists of the (1 1 6) and (0 0 8) planes in Sr_2IrO_4-9 T sample. (b) The HRTEM image which consists of the (1 1 6) and (0 0 4) planes in Sr_2IrO_4-0 T sample. (c) The enlargement of (a). (d) The enlargement of (b). (e) The HRTEM image of the (2 0 0) plane in Sr_2IrO_4-9 T. (f) The HRTEM image of the (2 0 0) plane in Sr_2IrO_4-0 T.

In order to make it clear, Fig. 2 (c) shows its enlargement. The weak dark regions in the (2 0 0) plane also appear in Fig. 2 (e) for Sr_2IrO_4-9 T. For comparison, Fig. 2 (b, d) shows the HRTEM images of Sr_2IrO_4-0 T which consists of (1 1 6) and (0 0 4) planes. Fig. 2 (f) depicts the HRTEM image in the (2 0 0) plane of Sr_2IrO_4-0 T. Such dark regions can not be observed in Sr_2IrO_4-0 T. The crystal lattice shows periodic behavior in each image. Furthermore, the HRTEM images indicate that the crystal structure of Sr_2IrO_4 is not changed even if the growth condition is different. The white circle which contains the dark region and background, as depicted in Fig. 2 (c), indicates that the crystal lattice is not changed in the dark regions.

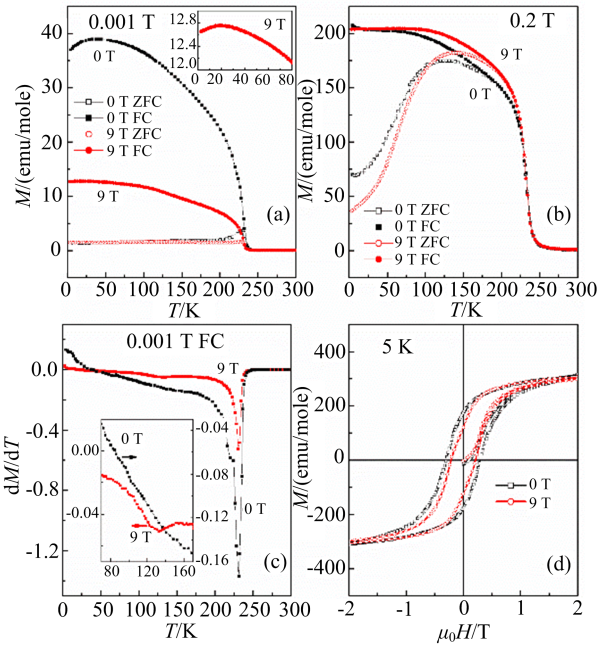

Fig. 3 Temperature dependence of the magnetization $M(T)$ for Sr_2IrO_4 (0 T and 9 T samples) under the magnetic field of 0.001 T (a) and 0.2 T (b). The inset in (a) displays the enlargement of M-T curve for Sr_2IrO_4-9 T from 0 K to 80 K. (c) dM/dT vs T of the FC curves under 0.001 T. The inset shows the enlargement of dM/dT (T) from 70 K to 170 K. (d) Field dependence of the magnetization $M(H)$ measured at 5 K.

Fig. 3 (a) depicts the M-T curves measured under the magnetic field of 0.001 T. It is obvious that the M-T curve for Sr_2IrO_4-0 T is far above the curve for Sr_2IrO_4-9 T below 240 K. For Sr_2IrO_4-0 T sample, M increases rapidly with cooling below 240 K, and it increases continuously below 210 K. Below 40 K, M drops with decreasing temperature, which demonstrates that the antiferromagnetic (AFM) interaction is enhanced. For Sr_2IrO_4-9 T sample, M increases slowly with cooling below the magnetic transition temperature. A

tiny dip is observed in Sr_2IrO_4-9 T at about 120 K, as shown in Fig. 3 (c) and the inset. Then M drops slightly with cooling below 40 K, as can be seen in the inset of Fig. 3 (a).

Figure 3 (b) gives the *M*-*T* curves measured under the magnetic field of 0.2 T. Obviously, the M-T curve for Sr_2IrO_4-9 T is raised greatly, and the magnetic transition region is overlapped with Sr_2IrO_4-0 T. Furthermore, the *M*-*T* curve for Sr_2IrO_4-9 T is a little higher than that of Sr_2IrO_4-0 T from 240 K to 50 K. The dip exhibited in Sr_2IrO_4-9 T and the drop of *M* below 40 K in Sr_2IrO_4-0 T disappear. As depicted by the *M*-*H* curves in Fig. 3 (d), the coercivity of Sr_2IrO_4-9 T is about 0.2 T, which is a little smaller than that of Sr_2IrO_4-0 T sample. These phenomena imply that the AFM interaction may be enhanced in the dark regions. Hence, the micromagnetism was further investigated by EMR.

In order to clear the origin of different behaviors in magnetization, we investigated the lattice dynamics by the infrared spectra. Fig. 4 gives the IR transmission spectra for Sr_2IrO_4-0 T and Sr_2IrO_4-9 T samples. As we know, Sr_2IrO_4 belongs to a distorted K_2NiF_4-type structure with the space-group $I4_1/acd$[2]. According to the group symmetry, peak 5 is classified to the bending mode A_{2u}, which is related to the modulation of Ir-O-Ir bond angle[13-15]. It can be seen that there is an important difference in the change of A_{2u} mode with decreasing temperature. For Sr_2IrO_4-0 T, the A_{2u} mode shows obvious blue shift with cooling from 300 K to 40 K, and then it only exhibits small shift below 40 K, as shown in Fig. 4 (c). But for Sr_2IrO_4-9 T, the blue shift of A_{2u} mode changes at 120 K. The blue shift of A_{2u} mode above 40 K for Sr_2IrO_4-0 T and 120 K for Sr_2IrO_4-9 T is due to the thermal contraction, and the bond angle of Ir-O-Ir keeps unchanged[3]. Below 40 K for Sr_2IrO_4-0 T and 120 K for Sr_2IrO_4-9 T, the shift of A_{2u} mode is induced by the decrease of Ir-O-Ir bond angle.

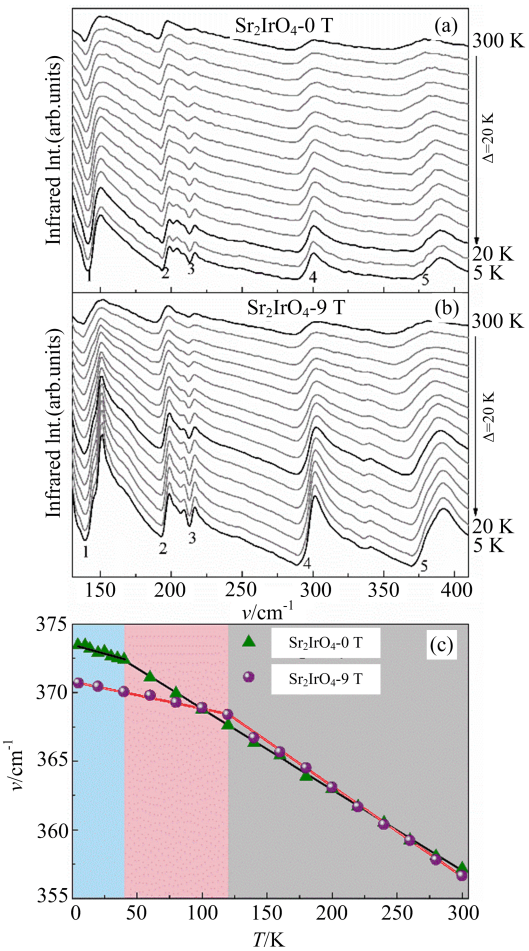

Fig. 4 Temperature-dependent infrared transmission spectra of (a) Sr_2IrO_4-0 T sample; (b) Sr_2IrO_4-9 T sample at selected temperatures from 300 K to 5 K. (c) The A_{2u} mode varies with temperature.

4 Discussion

Our experimental results reveal that the magnetic field of 9 T could be more favorable to the growth of pure phase, since only tiny amount of paramagnetic signals can be observed in the EMR spectra. As shown in Fig. 2 (a, c, e), some dark regions appear on the background of the homogeneous lattice in Sr_2IrO_4-9 T sample. Since these dark regions almost distribute regularly, which is depicted in Fig. 2 (a), they can not be introduced by the thickness nonuniformity of material. It is emphasized that the crystal lattice is continuous from the dark regions to the background, as depicted by the white circle in Fig. 2 (c) which includes

the dark region and background. This phenomenon means that the distribution of electron cloud may be changed in the growth of sample under the magnetic field of 9 T. The density of electron states could be increased in the dark regions and the light transmittance is weakened. So, the electromagnetic behavior of sample is affected directly by the increased density of electron states.

It is noted that the magnetic ground state of Sr_2IrO_4 is canted antiferromagnetic state, which produces a residual ferromagnetic component in the IrO2-plane[16,17]. Since the density of electron states increases in the dark regions of Sr_2IrO_4-9 T sample, the ordered interaction would be enhanced below 240 K. The antiferromagnetic interaction is also enhanced, and then the ferromagnetic component becomes weakened. Therefore, M of Sr_2IrO_4-9 T sample is much smaller than that of Sr_2IrO_4-0 T sample below 240 K, as can be seen in Fig. 3 (a). This phenomenon is also disclosed by the micromagnetism. As we know, the EMR signals are introduced by the canted magnetic order with $J_{eff}=1/2$ in Sr_2IrO_4 below the magnetic transition temperature. The increase of H_s indicates that the AFM interaction of system is enhanced with decreasing temperature. For Sr_2IrO_4-9 T, H_s is larger than that of Sr_2IrO_4-0 T at low temperature. Therefore the AFM interaction is stronger in Sr_2IrO_4-9 T comparing with Sr_2IrO_4-0 T.

Our IR results show that the bond angle ofIr-O-Ir decreases at 40 K for Sr_2IrO_4-0 T and 120 K for Sr_2IrO_4-9 T. Since the strength of DM interaction depends on the Ir-O-Ir bond angle, the ferromagnetic component decreases due to the reduction of Ir-O-Ir bond angle. So M should drop below 40 K for Sr_2IrO_4-0 T and 120 K for Sr_2IrO_4-9 T. For Sr_2IrO_4-0 T, M does decrease with cooling below 40 K, as depicted in Fig. 3 (a). But for Sr_2IrO_4-9 T, M does not show obvious drop below 120 K and it decreases slightly with cooling below 40 K. The AFM interaction should be enhanced below 120 K due to the reduction of Ir-O-Ir bond angle, as shown in Fig. 4 (b). On the other hand, the ferromagnetic component of system increases with decreasing temperature, which is determined by the intrinsic transition of $M\sim T$ in Sr_2IrO_4-0 T that M would increase with cooling from 240 K to 120 K, as can be seen in Fig. 3 (a). Therefore, the competition between them leads to a tiny dip which is observed at about 120 K. Below 40 K, M drops with decreasing temperature due to the intrinsic transition of $M\sim T$ in Sr_2IrO_4-0 T.

As depicted in Fig. 3 (b), the $M\sim T$ curve measured under 0.2 T for Sr_2IrO_4-9 T is raised greatly and it is almost consistent with that of Sr_2IrO_4-0 T. The increase of ferromagnetic component in the system may be due to the change which occurs to the orientation of the magnetic domains. Because the magnetic domains could be pinned by the impurities existing in Sr_2IrO_4-0 T, the coercivity of Sr_2IrO_4-0 T is larger than that of Sr_2IrO_4-9 T.

5 Conclusion

In summary, our experimental results indicate that the magnetic field of 9 T is favorable to the growth of pureSr_2IrO_4. Although the structure and crystal lattice of Sr_2IrO_4-9 T are the same with Sr_2IrO_4-0 T, the distribution of electron clouds is changed. The density of electron states for Sr_2IrO_4-9 T is increased in these dark regions on the background of Sr_2IrO_4-0 T, and the AFM interaction is enhanced, which leads to the great reduction of $M\sim T$ curve comparing with that of Sr_2IrO_4-0 T. For Sr_2IrO_4-0 T, the Ir-O-Ir bond angle decreases and the AFM interaction is enhanced below 40 K. But for Sr_2IrO_4-9 T, this reduction of Ir-O-Ir bond angle is raised to 120 K due to the increased electron density in the dark regions.

Acknowledgment

This work was supported by the National Natural Science Foundation of China through Grant nos. 11204288.

参 考 文 献

[1] S. J. Moon, M. W. Kim, K. W. Kim, Y. S. Lee, J. -Y Kim, J. -H Park, B. J. Kim, S. -J. Oh, S. Nakatsuji, Y. Maeno, I. Nagai, S. I. Ikeda, G. Cao, T. W. Noh, *Phys Rev B*, **74** (2006), 113104.

[2] G. Cao, P. Schlottmann , *Rep Prog Phys*, **81** (2018), 042502.

[3] M. Ge, S. Tan, Y. Huang, L. Zhang, W. Tong, L. Pi and Y. Zhang,*J Magn Magn. Mater*, **345** (2013), 13.

[4] M. Ge, T. F. Qi, O. B. Korneta, D. E. DeLong, P. Schlottmann, W. P. Crummett, G. Cao, *Phys Rev B*, **84** (2011), 100402(R).

[5] J. S. Lee, Y. Krockenberger, K. S. Takahashi, M. Kawasaki, Y. Tokura, *Phys Rev B*, **85** (2012), 035101B. .

[6] S. Calder, G. -X. Cao, M. D. Lumsden, J. W. Kim, Z. Gai, B. C. Sales, D. Mandrus, A. D. Christianson, *Phys Rev B*, **86** (2012), 220403(R).

[7] T. Han, Y. Wang, J. Yang, L. He, J. Xu, D. Liang, H. Han, M. Ge, C. Y. Xi, W. K. Zhu, C. Zhang and Y. Zhang,*Appl Phys Lett*, **109** (2016), 192409.

[8] F. Ye, X. Wang, C. Hoffmann, J. Wang, S. Chi, M. Matsuda, B. C. Chakoumakos, J. A. Fernandez-Baca,. G. Cao , *Phys Rev B*, **92** (2015), 201112(R).

[9] S. Marik, L. Lefevre, S. Fourcade, R. Decourt, O. Toulemonde , *J Alloy Compd*, **735** (2018), 1908.

[10] A. F. May, H. Cao, S. Calder, *Phys Rev Mater*, **2** (2018), 094406.

[11] P. Dong, X. Wang, J. Cheng, X. Yan , *Solid State Commun*, **296** (2019), 21.

[12] D. Haskel, G. Fabbris, M. Zhernenkov, P. P. Kong, C. Q. Jin, G. Cao, M. van Veenendaal, *Phys Rev Lett*, **109** (2012), 027204.

[13] S. J. Moon, H. Jin, W. S. Choi, J. S. Lee, S. S. A. Seo, J. Yu, G. Cao, T. W. Noh, Y. S. Lee, *Phys Rev B*, **80** (2009), 195110.

[14] M. F. Cetin, P. Lemmens, V. Gnezdilov, D. Wulferding, D. Menzel, T. Takayama, K. Ohashi, H. Takagi, *Phys Rev B*, **85** (2012), 195148.

[15] C. H. Sohn, Min-Cheol Lee, H. J. Park, Kyung Joo Noh, H. K. Yoo, S. J. Moon, K. W. Kim, T. F. Qi, G. Cao, Deok-Yong Cho, T. W. Noh, *Phys Rev B*, **90** (2014), 041105(R).

[16] G. Jackeli, G. Khaliullin, *Phys Rev Lett*, **102** (2009), 017205.

[17] H. Jin, H. Jeong, T. Ozaki, J. Yu, *Phys Rev B*, **80** (2009), 075112.